# Differential cross sections for single ionization of Li in collisions with fast protons and $O^{8+}$ ions

L. Gulyás
*Institute of Nuclear Research of the Hungarian Academy of Sciences (ATOMKI), H-4001 Debrecen, PO Box 51, Hungary*

S. Egri
*Department of Experimental Physics, University of Debrecen, 18/a Bem tér, H-4026 Debrecen, Hungary*

T. Kirchner
*Department of Physics and Astronomy, York University, 4700 Keele Street, Toronto, Ontario, Canada M3J 1P3*
(Received 16 September 2014; published 15 December 2014)

We study the process of single ionization of Li in collisions with $H^+$ and $O^{8+}$ projectile ions at 6-MeV and 1.5-MeV/amu impact energies, respectively. Using the frameworks of the independent-electron model and the impact parameter picture, fully (FDCS) and doubly (DDCS) differential cross sections are evaluated in the continuum distorted wave with eikonal initial-state approximation. Comparisons are made with the recent measurements of LaForge *et al.* [J. Phys. B **46**, 031001 (2013)] for the DDCS and Hubele *et al.* [Phys. Rev. Lett. **110**, 133201 (2013)] for the FDCS, respectively. For $O^{8+}$ impact inclusion of the heavy particle [nucleus-nucleus (NN)] interaction in the calculations is crucial and effects of polarization due to the presence of the projectile ion have also to be taken into account for getting very good agreement with the measured data. Our calculation reproduces the satellite peak structure seen in the FDCS for the Li($2s$) measurement, which we explain as being formed by a combination of the binary and NN interactions.

DOI: 10.1103/PhysRevA.90.062710 PACS number(s): 34.70.+e

## I. INTRODUCTION

The study of single and multiple ionization of simple atoms by fast bare ion impact provides an excellent opportunity to explore mechanisms leading to the breakup of few-body Coulomb systems [1–3]. In the last few decades, thanks to the development of cold-target recoil-ion momentum spectroscopy (COLTRIMS) [4], there have been very intense efforts to explore the different mechanisms in fine details; see [5–7] and references therein. The very recent implementation of laser cooling in a magneto-optical trap combined with a reaction microscope (MOTReMi) has opened up the possibility of studying collision processes with state-prepared target atoms [8].

Studying simple collision systems has the advantage of being able to get complete kinematic information on the processes experimentally. Fully differential cross sections can be determined, whose interpretations offer a real challenge for theoretical modeling. In recent years, intense discussions have been generated, e.g., on the role of the nucleus-nucleus (NN) interaction or on projectile coherence effects which remain hidden in most of the less differential measurements [9–11]. The decisive role of the NN interaction has also been demonstrated in a recent kinematically complete experiment for single ionization in an initial-state selective study of $O^{8+}$-Li($2s$),Li($2p$) collisions [12,13]. Significant initial state dependence has been reported for the doubly differential cross section as a function of electron energy and transverse momentum transfer. The experimental data were confronted with predictions from continuum distorted wave with eikonal initial state (CDW-EIS) calculations and, surprisingly, a classical description of the NN interaction provided the best agreement. In subsequent theoretical studies based on the close-coupling approach (CC) [14] and the coupled-pseudostate approximation (CP) [15] noticeable effects of the NN interaction have been confirmed and reasonable agreement between experiment and theory was concluded.

Distortion or polarization of an atomic electron orbital by other target electron(s) or by the incident charged particle is one of the most difficult tasks to deal with in the theoretical descriptions. The problem can be addressed in the distorted wave formalism [16] or in terms of a polarization potential [17]. To describe the polarization potential, several functional forms have been suggested [18–20]. All of them have the $V_{\rm pol} \approx \alpha/2r^4$ asymptotic behavior at large distances $r$ from the target, where $\alpha$ is the dipole polarizability constant. However, at shorter distances, the exact form of the potential is not available, which is the main reason for the existence of several analytical expressions. They are usually obtained by fits to experimental data or by using some reasonable assumption on the behavior of the potential at short distances. A large number of theoretical studies have been devoted to selecting and testing polarization potentials in the area of electron-atom scattering; see, e.g., [18–21] and references therein. However, only little is known about the effects of $V_{\rm pol}$ in heavy particle collisions, especially at high projectile energies.

In this contribution we apply the CDW-EIS method [22,23] to calculate the differential cross sections for single ionization of Li in collisions with 6-MeV $H^+$ and 1.5-MeV/amu $O^{8+}$ projectile ions and discuss results in comparison with experimental data of LaForge *et al.* [13] and Hubele *et al.* [12], and with available theoretical results. Using the independent electron picture the one-electron transition amplitudes are determined in the CDW-EIS model. Having the impact parameter dependent transition amplitudes the effects of the NN interaction are taken into account by a phase factor. No exact form of this factor is available, however, different assumptions imposed on it proved to be useful for exploring the mechanisms of the underlining processes. Special attention is paid to the role of $V_{\rm pol}$. Different analytical forms are applied

 

and a characteristic role of $V_{\rm pol}$ is found at large momentum transfer values.

The article is organized as follows. In Sec. II we summarize the main points of our theoretical description. In Sec. III the results are discussed. A summarizing discussion is provided in Sec. IV. Atomic units characterized by $h = m_e = e = 4\pi\epsilon_0 = 1$ are used unless otherwise stated.

## II. THEORY

In order to reduce the very challenging many-electron treatment to a much simpler one-electron description we consider only one electron in Li as active over the course of the collision while the others remain bound to their initial state. The nonactive electrons are taken into account by an effective potential $V_{\rm Li}$ that represents the interactions in the $(1s^2 2s)$ ground-state configuration. This potential is obtained from the exchange-only version of the optimized potential method (OPM) of density functional theory, i.e., it includes the electron nucleus Coulomb interaction, screening, and exchange terms exactly and exhibits the correct $-1/r_T$ behavior, but it neglects electron correlation ($\mathbf{r}_T$ denotes the position vector of the electron relative to the target nucleus) [24]. The above assumption on the description of the target is the essential point in the application of the independent electron model (IEM) where electrons are considered to evolve independently and it enables us to simplify the treatment of a many-electron collision problem to a three-body system [2].

In the following we consider a three body-collision, where a bare projectile ionizes a target initially consisting of a bound system of an electron and a core represented by the $V_{\rm Li}$ interaction potential. Furthermore, we apply the impact parameter method, where the projectile follows a straight-line trajectory $\mathbf{R} = \boldsymbol{\rho} + \mathbf{v}t$, characterized by the constant velocity $\mathbf{v}$ and the impact parameter $\boldsymbol{\rho} \equiv (\rho, \varphi_\rho)$ [25]. The one-electron Hamiltonian has the form

$$h(t) = -\frac{1}{2}\Delta_{\mathbf{r}_T} + V_{\rm Li}(|\mathbf{r}_T|) - \frac{Z_P}{|\mathbf{r}_P|}, \tag{1}$$

where $\mathbf{r}_P$ denotes the position vector of the electron relative to the projectile nucleus having nuclear charge $Z_P$. The single-particle scattering equation is solved within the framework of the CDW-EIS approximation, where unperturbed atomic orbitals in both the incoming and outgoing channels have been evaluated on the same $V_{\rm Li}$ potential; see Refs. [16,22,23,26] for more details. Here we note that a similar formalism, including transition amplitudes from a basis generator method calculation, was used in our recent study of excitation and ionization in the 1.5-MeV/amu $O^{8+}$-Li collision system [27].

The doubly differential cross section (DDCS) differential in energy of the emitted electron $E_e$ [$=k_e^2/2$; $\mathbf{k}_e \equiv (k_e, \theta_e, \varphi_e)$ is the electron momentum] and in the transverse component [$\boldsymbol{\eta} \equiv (\eta, \varphi_\eta)$] of the projectile's momentum transfer $\mathbf{q} = \mathbf{k}_i - \mathbf{k}_f = -\boldsymbol{\eta} + \Delta E/v$ is given as

$$\frac{d\sigma^2}{dE_e d\eta} = k_e \eta \int_{-1}^{+1} d(\cos\theta_e) \int_0^{2\pi} d\varphi_e \int_0^{2\pi} d\varphi_\eta |\mathcal{R}_{i\mathbf{k}}(\boldsymbol{\eta})|^2, \tag{2}$$

where $\Delta E = E_e - \varepsilon_i$, $\varepsilon_i$ is the binding energy of the electron in the initial state, $\mathbf{k}_{i(f)}$ stands for the projectile momentum before (after) the collision, and $\mathcal{R}_{i\mathbf{k}}(\boldsymbol{\eta})$ is the transition matrix.

In Eq. (2) the projectile's momentum transfer and consequently the projectile scattering is defined by the interaction of the projectile with the active electron. However, the scattering of the projectile also depends on its interaction with the target core (so-called NN interaction). We approximate this interaction by using the potential

$$V_{\rm NN}(R) = Z_P Z_T / R + V_s(R) + V_{\rm pol}(R), \tag{3}$$

where

$$V_s(R) = Z_P \sum_{i=1}^{2} \left\langle \psi_{1s}^i \right| - 1/|\mathbf{R} - \mathbf{r_i}| \left| \psi_{1s}^i \right\rangle \tag{4}$$

describes the interaction between the projectile and the passive electrons. In (4) $\psi_{1s}^i$ is approximated by a hydrogenlike wave function ($\psi_{1s}^i = N_i e^{-z_e^i r_T}$) with effective charge $z_e^i(=2.65)$ (Slaters's rule [28]). Taking $z_e^1 = z_e^2$, we obtain

$$V_s(R) = -2Z_P[1/R - [(1 + z_e R)/R]e^{-2z_e R}]. \tag{5}$$

On the accuracy of (5) we note that we have evaluated $V_s(R)$ with the Li$(1s)$ OPM orbital and have compared it with (5). The difference is very small, which is supported by the fact that the OPM Hartree potential $V_H^{\rm OPM}$ for the $Li^+(1s^2)$ configuration has the limit $\lim_{R\to 0} V_H^{\rm OPM}(R) \to 5.375$ which corresponds to $z_e = 2.687$. It can be checked that $\lim_{R\to 0} V_{NN}(R) \to 3Z_P/R$ and $\lim_{R\to\infty} V_{NN}(R) \to Z_P/R$ for $Z_T = 3$.

$V_{\rm pol}(R)$ in (3) accounts for the (adiabatic) polarization or distortion of the core electrons by the incident charged particle [17,21]. Its use is based on the idea that the electric field of the projectile at distance $R$ gives rise to an instantaneous (first-order) distortion of the core-electron orbitals, thereby modifying the interaction of those electrons with the projectile. Polarization potentials have been used in many studies up to fairly high projectile energies [18,20,21,29]; in particular in [15], in which the CP method was applied to the collision system considered in this work. Different types of analytical approximations are available for $V_{\rm pol}(R)$ and we consider the following three frequently used forms:

$$V_{\rm pol}(R) = -\frac{\alpha Z_P^2}{2(R^2 + d^2)^2}, \tag{6}$$

where $\alpha$ is the atomic dipole polarizability parameter [20] and $d$ is a "cutoff" parameter whose value is taken as the average radius of the $Li^+(1s^2)$ ion ($d = 0.57$ a.u. for the present case) [19];

$$V_{\rm pol}(R) = -\frac{\alpha Z_P^2}{2R^4}[1 - \exp(-(R/r_d)^6)], \tag{7}$$

with $r_d = 0.47$ [30]; and

$$V_{\rm pol}(R) = -\frac{\alpha Z_P^2}{2R^4}[1 - e_n(\xi)\exp(\xi)]^m, \tag{8}$$

with $\xi = R/r_o$ where $e_n(\xi)$ is the truncated exponential function $e_n = \sum_{i=0}^{n} (\xi)^i / i!$, $r_o = 0.116$, $m = 6$ and $n = 2$ [18]. All these polarization potentials have the form $V_{\rm pol}(R) \approx -\alpha/2R^4$ at large distances and differ in the short-range limit due to

the cutoff parameters or functions which contain parameters estimated on some reasonable assumptions.

Effects of the NN interaction on the scattering process can be investigated by solving the Schrödinger equation for the Hamiltonian (1) with inclusion of the potential (3). However, the solution simplifies remarkably if one considers that (3) depends on $R$ alone and so $V_{NN}$ can be removed from (1) by a phase transformation. The transition matrix $\mathcal{R}_{i\mathbf{k}}(\boldsymbol{\eta})$ that takes the internuclear interaction into account can then be expressed as [25]

$$\mathcal{R}_{i\mathbf{k}}(\boldsymbol{\eta}) = \frac{1}{2\pi}\int d\boldsymbol{\rho} e^{i\boldsymbol{\eta}\cdot\boldsymbol{\rho}} a_{i\mathbf{k}}(\boldsymbol{\rho}) \tag{9}$$

with $a_{i\mathbf{k}}(\boldsymbol{\rho}) = e^{i\delta(\rho)}\mathcal{A}_{i\mathbf{k}}(\boldsymbol{\rho})$, where $\mathcal{A}_{i\mathbf{k}}(\boldsymbol{\rho})$ is the transition amplitude calculated without the internuclear interaction, and the phase due to (3) is expressed as

$$\delta(\rho) = -\int_{-\infty}^{+\infty} dt\, V_{NN}(R(t)). \tag{10}$$

## III. RESULTS

### A. Doubly differential cross sections for the ionization of Li (2$s$) and Li(2$p$)

In Figs. 1–7 we compare our CDW-EIS results of $d\sigma^2/dE_e d\eta$ for proton and $O^{8+}$ impact on Li(2$s$) and Li(2$p$) with measurements of LaForge *et al.* [13] and Hubele *et al.* [12] for the electron ejection energies of 2, 10, and 20 eV. The experimental data of [13] and [12] are not on the absolute scale, only the relative normalization was fixed for different $E_e$ and for Li(2$p$) relative to Li(2$s$). Following previous works [13–15] we have fixed the absolute scale in the figures by normalizing the data to our CDW-EIS cross sections for 2-eV ejection from Li(2$s$) at $\eta = 0.65$ a.u.

#### 1. $H^+$ projectile impact at 6 MeV

It is clear from panels (a) and (b) of Figs. 1–3 that the role of the internuclear interaction is negligible in the whole range of $\eta$ where the measurements have been taken when the projectile is a 6-MeV proton. This has also been noted in [13,15]. We have also evaluated cross sections with $V_{NN} = Z_P Z_{\text{eff}}/R$, and $Z_{\text{eff}} = 3.0$, 1.0, and 1.35. The first and second choice correspond to a close and a distant collision of the heavy particles respectively and the last one is an intermediate situation in which $Z_{\text{eff}}$ is obtained from Slater's screening rule. DDCS's evaluated with these NN interactions are not presented in panels (a) and (b) of Figs. 1–3 as they are almost the same as those obtained with or without (3). The indifference of the DDCS to the form of NN interaction is explained by the almost constant character of the internuclear phase over the region of $\rho$ [see (10)], where $\mathcal{A}_{i\mathbf{k}}(\boldsymbol{\rho})$ has significant values.

Panels (a) and (b) of Figs. 1–3 also show results of CDW-EIS calculations by LaForge *et al.* [13]. Their results are almost the same as the present ones for all $E_e$'s when the shapes of the curves are considered. Slight differences appear mostly at small $\eta$ values and for those $\eta$'s where the DDCS's have

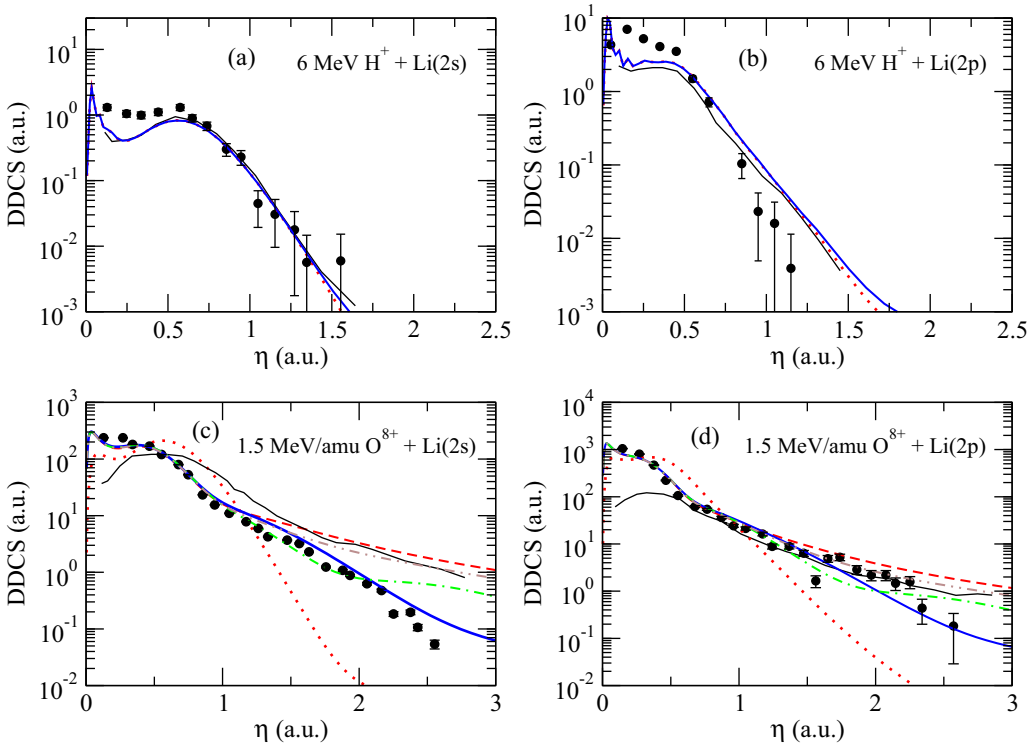


FIG. 1. (Color online) DDCS for single ionization of Li(2$s$) and Li(2$p$) by 6-MeV $H^+$ (upper panels) and 1.5-MeV/amu $O^{8+}$ (lower panels) impact as a function of $\eta$ for $E_{el} = 2$ eV. Theories: present results, dotted red lines represent calculations without the NN interaction; calculations with NN interaction where $V_p = 0$ are dashed red lines and where $V_p$ is given by (6) with $d = 0.57$ thick solid blue lines; (7) are dot-dashed green lines; (8) are dot-dot-dashed brown lines; see the text. Black thin solid curves are CDW-EIS calculations by LaForge *et al.* with classical NN interaction [13]. Experiment: • from [13] as renormalized recently [32].

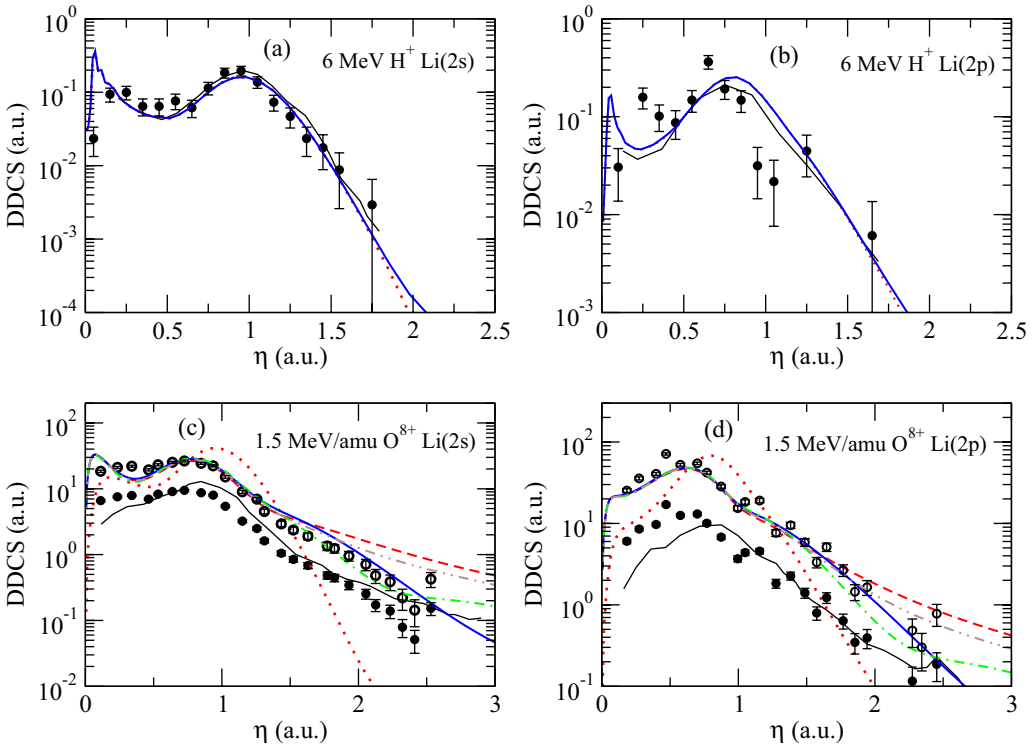


FIG. 2. (Color online) Same as Fig. 1 but for $E_{el} = 10$ eV. ○ experimental data of LaForge *et al.* [13,32] normalized for best visual fit.

maxima. As noted above, the NN interaction is negligible for proton impact, so the difference between the two CDW-EIS calculations lies in the description of the target orbitals. However, it must be noted that the above discrepancies are within the experimental uncertainties.

### 2. $O^{8+}$ projectile impact at 1.5 MeV/amu

The picture becomes more complicated for $O^{8+}$ ion impact; see the lower panels [(c) and (d)] in Figs. 1–3. The role of the internuclear interaction is more evident for this projectile than for the $H^+$ ion. DDCS's evaluated with and without the NN

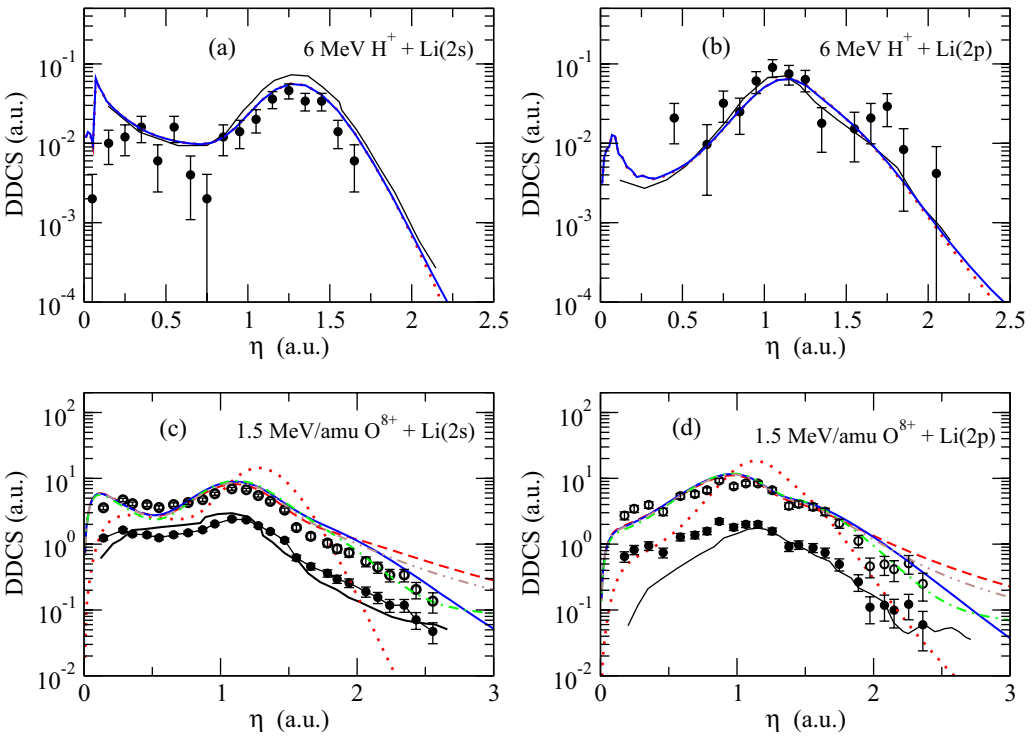


FIG. 3. (Color online) Same as Fig. 2 but for $E_{el} = 20$ eV.

interaction differ considerably. $\delta(\rho)$, see (10), oscillates rapidly with $\rho$ when $Z_p = 8$ and the DDCS is sensitive to the form of the NN interaction. Let us first consider results evaluated with the NN interaction where the polarization potential is set to zero, $V_{\rm pol} = 0$ in (3). Compared to the measurements, calculations with the more sophisticated screening potential (4) present reasonable agreement. For all $E_e$ and for both $2s$ and $2p$ the agreement is very good from medium to low $\eta$ values and discrepancies appear only in the large $\eta$ region where the calculations overestimate the measurements. Calculations with $V_{NN} = Z_P Z_T/R$ (not shown in the figures) fail in almost the entire range of $\eta$ showing the important screening role of the passive electrons. At the same time when the internuclear interaction is taken into account by $V_{NN} = Z_P/R$ the calculations result in DDCS which are very similar to those obtained with (3), for the case of $V_{\rm pol} = 0$. This becomes clear if we consider the range of $\rho$ over which $\mathcal{A}_{i\mathbf{k}}(\boldsymbol{\rho})$ has significant values. This range extends to $\rho \approx 25$–$30$ a.u., however, $V_{NN}(R)$ of (3) reaches its asymptotic limit and behaves as $Z_P/R$ when $\rho \geqslant 1$–$2$ a.u. So the DDCS is governed by the asymptotic form of the NN interaction in almost the entire range of impact parameters. Here we note that similar findings on the role of $V_s$ in (3) were reported in [31] for the case of 100 MeV/amu $C^{6+}$ and 1 GeV/amu $U^{92+}$ impact on helium.

Let us now consider results obtained with (3), i.e., the full form of the NN interaction potential, in which $V_{\rm pol}$ is also taken into account. It is clear from the lower panels of Figs. 1–3 that $V_{\rm pol}$ has a negligible effect at low $\eta$ values, however, it plays a drastic role in the large-$\eta$ region. Very good results are found in the whole $\eta$ region for all electron energies when $V_{\rm pol}$ takes the form (6). Taking (7) for $V_{\rm pol}$ also results in good agreement below $\eta \leqslant 2$ a.u., while above this value these calculations overestimate the experiment. We note that a $V_{\rm pol}$ the same as or similar to that in Eq. (7) was probably used in [15], which is supported by the fact that the results reported in that work are consistent with the present ones. Results with $V_{\rm pol}$ of (8) are very close to those obtained with $V_{\rm pol} = 0$.

As for the case of $H^+$ impact, panels (c) and (d) of Figs. 1–3 also present the CDW-EIS results of LaForge *et al.* [13]. Their CDW-EIS calculations, in which the NN interaction was taken into account classically, fail to reproduce the measured data mostly at low $\eta$ values. LaForge *et al.* [13] also presented results where the NN interaction was accounted for quantum mechanically in terms of the eikonal approximation. However, they found that the classical treatment was more adequate especially at large $\eta$ with increasing $E_e$. Given the good results of the present calculations we see no reason to perform similar calculations with a classical inclusion of the NN interaction.

Hitherto, we have discussed DDCS results by considering only their shapes. Obviously, confronting a calculation with a measurement that is lacking an absolute normalization might influence the assessment of the validity of the theory. In Figs. 1–3, we have normalized the measured DDCS to our calculation at $\eta = 0.65$ a.u. for Li($2s$) at $E_e = 2$ eV. Normalization at a different $\eta$ might modify the judgment of the theory. This is especially true when relative cross sections for the different ejection energies are considered. These comments mainly apply to the case of $O^{8+}$ impact; see Figs. 2 and 3, where shifted experimental data showing the "best visual fit" are also presented with open symbols. The shifts correspond to factors of about 2–5 depending on the collision parameters. A similar drift in the relative normalization of the DDCS for $O^{8+}$ impact has also been noted in [15].

### 3. *Exploring the role of the polarization potential*

Deviations of DDCS's at large $\eta$ obtained with the different forms of $V_{\rm pol}$ can be explored by considering the potentials and the internuclear phases ($\delta_{\rm pol}$) evaluated only on them [see (10)]. Figure 4(a) shows $V_{\rm pol}$ of (6)–(8) as a function of $t$ for three different $\rho$ values; note that $\rho$ and $t$ are related by $\mathbf{R} = \boldsymbol{\rho} + \mathbf{v}t$. This figure indicates that considerable differences among the potentials appear only for $\rho \leqslant 1$ a.u. $V_{\rm pol}$ of (6) contains a cutoff parameter for which we take the $1s$ shell radius $d = 0.57$ a.u. Different criteria for $d$ have also been proposed in [21] and [19]. They result in $d = 0.3$ and 0.93, respectively. $V_{\rm pol}$ evaluated with these values of $d$ are not represented in Fig. 4(a). However, deviations related to the use of different $d$ parameters in (6) can be assessed from Fig. 4(b). Figure 4(b) presents $\delta_{\rm pol}$ evaluated with $V_{\rm pol}$ of (6) using three different values for $d$ in comparison with those obtained from $V_{\rm pol}$ of (7) and (8). It is clear that the phases are the same for all forms of polarization potential when $\rho \geqslant 1$, however, the deviations are significant at small $\rho$ due to different cutting procedures in (6) and different forms of $V_{\rm pol}$. Apart from the very low $\rho$ region, which is unimportant for the DDCS, $V_{\rm pol}$ of (6) with $d = 0.3$ provides nearly the same $\delta_{\rm pol}$ as that of (7). At the same time $\delta_{\rm pol}$ provided by $V_{\rm pol}$ of (6) with $d = 0.93$ and of (8) have very small values. This fact explains the small differences between DDCS's with (8) and without polarization potential observed in panels (c) and (d) of Figs. 1–3. It is also obvious that deviations in $\delta_{\rm pol}$ and so in $V_{\rm pol}$ are manifested in the DDCS in the large $\eta$ region. This can be observed in Fig. 5 where the DDCS evaluated with different forms of $V_{\rm pol}$ is presented for $O^{8+} + {\rm Li}(2s)$ collsions for $E_e = 2$ eV.

In [15] ionization of Li was discussed within the framework of the coupled pseudostate (CP) model. Their results show similar good agreement with the measurement as the present ones at low and medium $\eta$ values when the shapes of the DDCS's are considered. A similar study within the framework of the time-dependent close-coupling (TDCC) method was performed for $O^{8+}$ impact only in [14]. Reasonable agreement, especially for the Li($2p$) target was observed. Results of these calculations are not included in Figs. 1–3 for the sake of clarity. However, in Figs. 6 and 7 we give a comparison of the present, the CP, and the TDCC results for some selected collision parameters. In Fig. 6 we compare the present DDCS results for $O^{8+} + {\rm Li}(2s)$ collisions at $E_e = 2$ eV with the CP and the TDCC results. The DDCS from the TDCC calculation is normalized to the present data at $\eta = 0.65$ a.u. while those from the CP is shown on an absolute scale. In [15] the polarization potential was probably given by (7) and the agreement between their and our results obtained with $V_{\rm pol}$ of (7) is good except around $\eta = 2$ a.u. In [14] the NN interaction was taken into account by the Coulomb repulsion with an effective charge and those results seem to be comparable to our results without $V_{\rm pol}$.

Similarly good agreement between our and the CP results of [15] can be observed in Fig. 7 showing the DDCS for

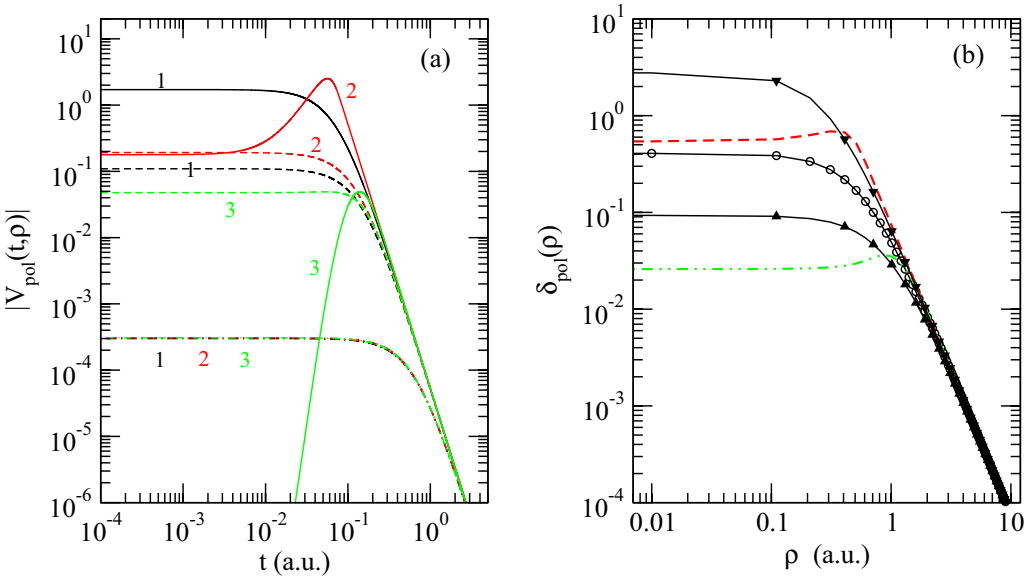


FIG. 4. (Color online) (a) $|V_{pol}(R)|$ of (6) ($d = 0.57$), (7) and (8) represented by curves 1, 2, and 3 as functions of $t = \frac{1}{v}\sqrt{R^2 - \rho^2}$ for $\rho = 0.1$, 1.0, and 5.0 a.u. with solid, dashed, and dot-dashed lines respectively. (b) Internuclear phases (10) are shown due to $V_{pol}$ of (6) for $d = 0.57$, 0.3, and 0.93 as solid lines with circle, triangle down, and triangle up symbols; of (7) with dashed red; and of (8) with dot-dot-dashed green lines.

1.5 MeV/amu $O^{8+}$ Li($2p_{0,1}$) collisions at $E_e = 20$ eV. It is seen that CP and CDW-EIS calculations agree well in the binary region and slight discrepancies appear at low and high $\eta$ values [see Fig. 7(a)]. It is important to note the good agreement on the absolute scale. Figure 7(b) shows results of calculations in which the NN interaction is neglected. Besides the present CDW-EIS results, results of a first Born (B1) calculation performed by us and a B1 calculation from [15] are also presented. The two B1 calculations are in very good agreement and differ from the CDW-EIS cross sections only at $\eta \leqslant 0.5$ a.u. values. This tells us that, except for the very low region of $\eta$, the collision with the $O^{8+}$ projectile is still in the B1 regime. Including the NN interaction in a treatment where $\mathcal{A}_{i\mathbf{k}}(\boldsymbol{\rho})$ is evaluated in B1 yields a similar good account of the measurements as the CDW-EIS model (except at very low $\eta$).

### B. Fully differential cross sections

A more detailed analysis can be performed on the level of the fully differential cross section (FDCS),

$$\frac{d\sigma^3}{dE_k d\Omega_e d\Omega_f} = k_e |\mathcal{R}_{i\mathbf{k}}(\boldsymbol{\eta})|^2, \tag{11}$$

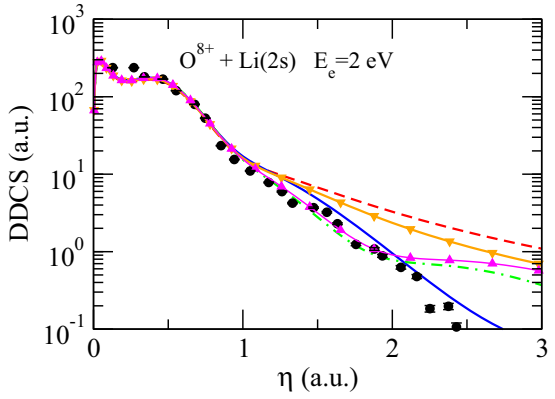


FIG. 5. (Color online) DDCS for single ionization of Li($2s$) by 1.5 MeV/amu $O^{8+}$ impact as a function of transverse momentum transfer for $E_e = 2$ eV. Present calculations including the NN interaction with $V_{pol} = 0$ are represented as dashed red and with $V_{pol}$ given by (6) with $d = 0.57$ as solid blue, $d = 0.3$ as solid pink + triangle up, $d = 0.93$ as solid orange + triangle down, and by (7) as dot-dashed green lines, respectively. • experimental data from [13] as renormalized recently [32].

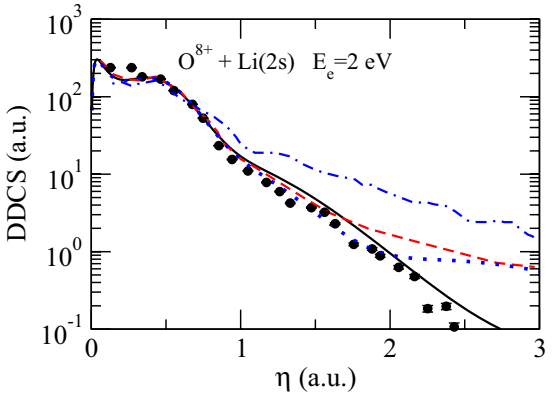


FIG. 6. (Color online) DDCS for single ionization of Li($2s$) by 1.5-MeV/amu $O^{8+}$ impact as a function of transverse momentum transfer for $E_e = 2$ eV. Present calculations including the NN interaction with $V_{pol}$ given by (6) with $d = 0.57$ and 0.3 are the solid black and dotted blue lines, respectively. Dashed red and dot-dashed blue lines are the CP and TDCC calculations from [15] and [14] (results from [14] are normalized to the present data at $\eta = 0.65$ a.u.). • experimental data from [13] as renormalized recently [32].

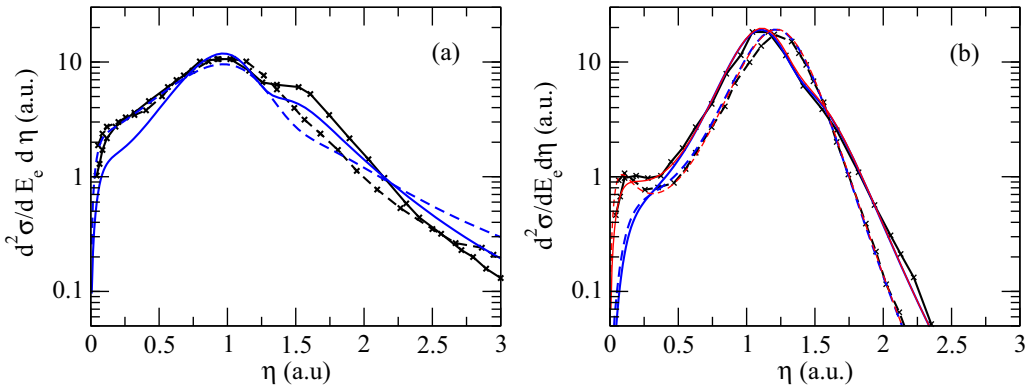


FIG. 7. (Color online) DDCS for single ionization of Li($2p_0$) (dashed lines) and Li($2p_1$) (solid lines) by 1.5 MeV/amu $O^{8+}$ impact as a function of $\eta$ for $E_e = 20$ eV with (a) and without (b) internuclear interaction. In (a), blue lines present CDW-EIS results and black lines with crosses are CP results from [15]. In (b) blue thick and red thin lines present CDW-EIS and B1 results, respectively, black lines with crosses are B1 results from [15].

where $d\Omega_f(\theta_f,\phi_f)$ and $d\Omega_e(\theta_e,\phi_e)$ denote the solid angles for the scattered projectile and emitted electron, respectively.

Figure 8 presents FDCS's for 1.5 MeV/amu $O^{8+}$-Li($2s,2p$) collisions as functions of $\phi_e$ when $\theta_e = 90^\circ$, $E_e = 1.5$ eV, and $q$ was set to 0.3 and 1.0 a.u. for $2p$ and $2s$, respectively. The $y$-$z$ plane is fixed by the incoming and scattered projectile's momenta with the positive $z$ axis pointing into the incident projectile direction. This Cartesian coordinate system is completed with an $x$ axis to form a right-handed system. $\phi_e$ is measured in the normal way with respect to the $x$ axis, that is Fig. 8 presents electron ejection cross sections in a plane perpendicular to the projectile direction. Let us first discuss results obtained with different forms of the polarization potential.

### 1. *Effects of polarization in the ionization of Li(2s) and Li(2p) at different q*

Calculations for Li($2p$) are carried out for $q = 0.3$ a.u. and as can be expected the cross sections are not very sensitive to the form of the $V_{\rm pol}$ interaction [only NN with (6) are presented in Figs. 8(a) and 8(b)]. At the same time for Li($2s$) where $q = 1$ a.u., see Fig. 8(c), the FDCS is very sensitive to the form of $V_{\rm pol}$. The calculation with (6) for the polarization potential, which showed a good account of the DDCS (see Figs. 1–3), reproduces the main characteristics of the measured distribution, however, it has defects when finer details are considered. Calculations with other forms of $V_{\rm pol}$ are less satisfactory. Calculations performed with an NN interaction potential using the effective target ion charge $Z_{\rm eff} = 1.0$ reveal that the collision parameters of Fig. 8 correspond to the distant collision regime. Similar calculations with $Z_{\rm eff} = 1.34$ reveal better agreement in shape, but a further increase of $Z_{\rm eff}$ cannot be justified as it adversely affects the absolute values of the cross section. A detailed analysis shows that the relative magnitudes of the peaks in Fig. 8(c) depend strongly on the character of the transition amplitude at around $\rho \approx 1$ a.u., where the polarization potentials change drastically due to the cutting procedures. Figure 8 shows also CP results of [15] which, especially for Li($2s$) are in better agreement with the experiment than the present calculations. Differences between the CP and CDW-EIS results appear not only in the shapes

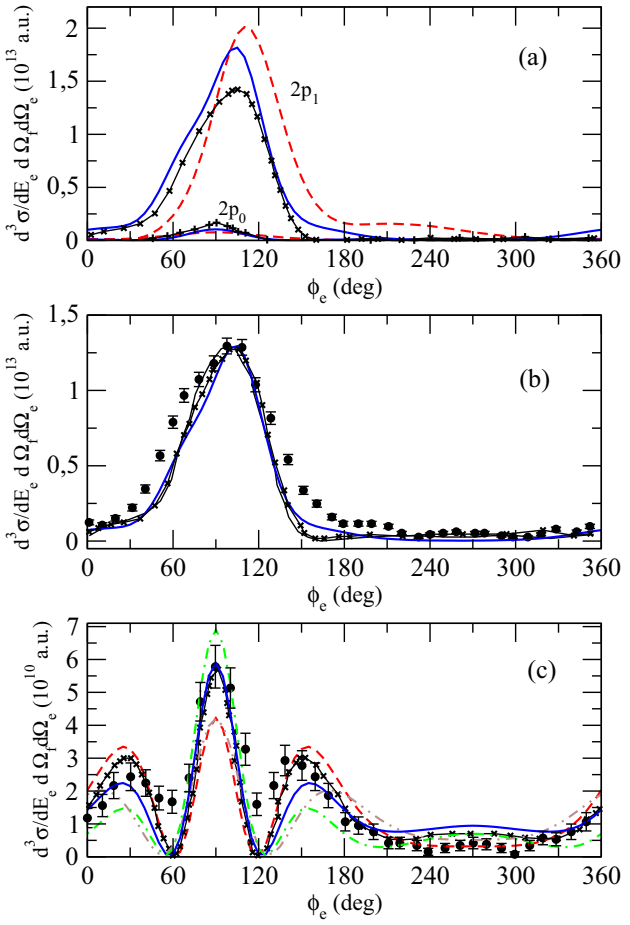


FIG. 8. (Color online) Fully differential cross section for single ionization of Li($2s,2p$) by 1.5-MeV/amu $O^{8+}$ impact as a function of $\phi_{el}$ for fixed $q$, $\theta_{el} = 90^\circ$ and $E_{el} = 1.5$ eV. (a) $2p_0$ and $2p_1$ for $q = 0.3$ a.u. (b) $0.3{\rm Li}(2p_0) + 0.7{\rm Li}(2p_1)$ for $q = 0.3$ a.u. (c) Li($2s$) for $q = 1.0$ a.u. Results of present calculations with NN interaction where $V_{\rm pol} = 0$ are dashed red lines and where $V_{\rm pol}$ is given by (6) are thick solid blue lines; (7) are dot-dashed green lines; (8) are dot-dot-dashed brown lines; see the text. Thin solid lines with crosses are the CP results from [15], in (b) and (c) the CP results are multiplied by 1.2. Circles and thin black solid lines are experimental and theoretical CDW-EIS results from [12].

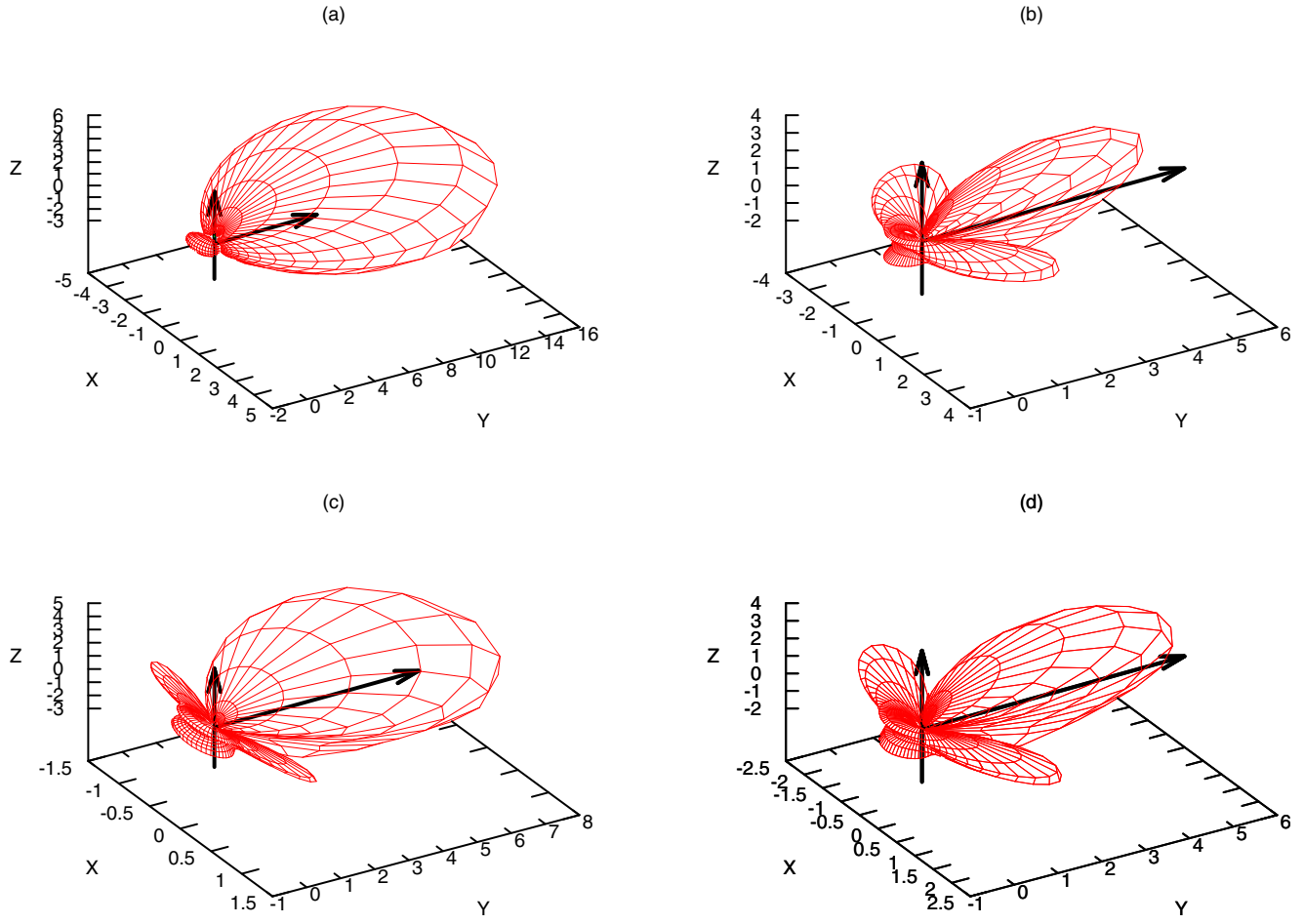


FIG. 9. (Color online) Spherical plot of the fully differential cross section for single ionization of Li($2s$) by 1.5 MeV/amu $O^{8+}$ impact for $q = 1.0$ a.u. and $E_{el} = 1.5$ eV. Calculations without (a) and with NN interaction where $V_{\rm pol}$ is given by (6) (b), (7) (c), (8) (d). The axes are in arbitrary units and the arrow pointing to toward the $+y$ direction denotes **q**.

of the FDCS's but also on the absolute scale. The latter is unexpected if one recalls the good account of the DDCS by both methods; see Fig. 5. We think that the observed discrepancy is related to the slightly different account of the NN interaction in the two calculations and this difference is probably emphasized with the decrease of $E_e$.

Figure 9 shows the fully differential angular distribution of electrons ejected in 1.5 MeV/amu $O^{8+}$–Li($2s$) collisions. $E_e$ is fixed at 1.5 eV and $q = 1.0$ a.u. Figure 9(a) presents the FDCS evaluated without internuclear interaction, while Figs. 9(b)–9(d) are obtained from calculations including the NN interaction with $V_{\rm pol}$ of (6), (7), and (8), respectively. Considerable differences can be observed between results with and without NN interaction. The more characteristic differences are the sharpening of the FDCS in the direction of **q** (positive $y$ axis) and the appearance of the wings in the $\pm x$ directions (perpendicular to the scattering plane) caused by the NN interaction. It is obvious from Fig. 9 that the two small peaks in Fig. 8(c) at $\phi \approx 30^\circ$ and $150^\circ$ are due to the wings whereas calculations without NN interaction only give rise to the centroid peak at $\phi = 90^\circ$. This has already been reported in [12] and [15]. At the same time considerable discrepancies are visible among results with different $V_{\rm pol}$. The node of the $2s$ orbital is at around $r_T \approx 1$ a.u. This is the distance where the differences in the polarization potentials are emphasized. Moreover, the phase due to $V_{\rm pol}$ affects the full NN phase only for $\rho \leqslant 1$ a.u. Accordingly, the strong variation of the FDCS with $V_{\rm pol}$ supports the idea that the shape of the wings is determined by the low $\rho$ character of the NN interaction.

Weaker deviations appear between calculations with and without NN interaction for the Li($2p$) ionization FDCS at $q = 0.3$ a.u., see Fig. 10. This FDCS is not symmetric with respect to the collision plane even for the calculation without NN interaction and the NN interaction further emphasizes this asymmetry.

### 2. *Satellite peaks in the ionization of Li(2s)*

Finally let us turn our attention to the satellite peak structure or the presence of the wings in the FDCS of Figs. 8(c) and 9, respectively. First of all we note that slow electrons are usually ejected in distant collisions between the projectile and target, where the three-body dipole interaction dominates [1]. At the same time for high impact velocities and large projectile charges the two-body binary encounter mechanism plays an important role and manifests itself as a sharp peak at $\theta_e \approx 90^\circ$ in the angular distribution. This is well seen in Fig. 11(a) where the DDCS versus $\theta_e$ is presented for $E_e = 1.5$ eV.

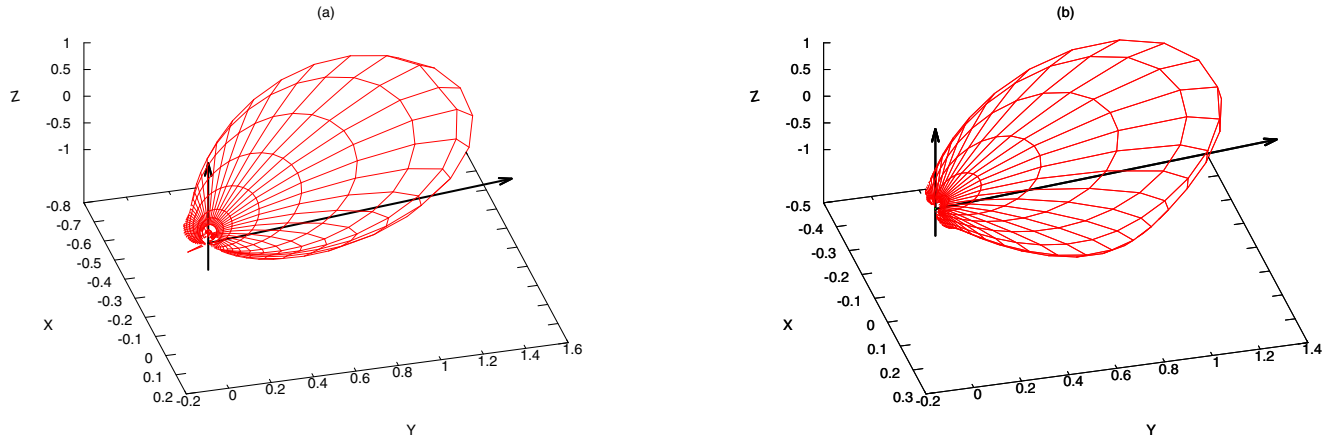


FIG. 10. (Color online) Spherical plot of the fully differential cross section for single ionization of $0.3\mathrm{Li}(2p_0) + 0.7\mathrm{Li}(2p_1)$ by 1.5 MeV/amu $O^{8+}$ for $q = 0.3$, and $E_{el} = 1.5$ eV. Left panel without, right panel with NN interaction where $V_{\mathrm{pol}}$ is given by (6). The axes are in arbitrary units and the arrow pointing to toward the $+y$ direction denotes **q**.

Results only due to the dipole interaction are derived from a CDW-EIS calculation where only the $l = 0,1$ partial waves from the expansion of the wave function for the final state have been taken into account [22]. The definite role of the binary mechanism is well seen at $\theta_e \approx 90^\circ$ in the figure. The FDCS's obtained only with the dipole interaction and with all interaction terms (including dipole and binary) are displayed in Fig. 11(b). This figure shows that the multiple peak structure in the FDCS appears only when binary and NN interactions are taken into account in the calculation. The binary interaction describes a head-on collision between the electron and the projectile, which obviously is important in the region where the electron density is significant. Test calculations demonstrated that the multiple peak structure reduces to a single peak characteristic of the projectile-electron interaction, when the NN interaction is neglected in a $\rho = [1\text{–}5]$ a.u. window in the calculation. This region of $\rho$ is comparable to the extension of the electron cloud for the $2s$ orbital. Moreover, we have performed calculations where $Z_p$ in the NN interaction has been varied. No satellite peaks are obtained for $Z_p \leqslant 3$, for which the shape of the FDCS is almost the same as in a calculation without the NN interaction. An analysis of the classical deflection function revealed that the impact parameter that corresponds to Coulomb scattering of the projectile (with $Z_p = 8$) from the target nucleus at $q = 1$ a.u. is at $\rho \approx 2.5$ a.u. For $Z_p = 1$ this region shifts to the much lower value $\rho \approx 0.2$ a.u. where the electron density is negligible. These results confirm the idea that the presence of the satellite peak or the wing structure in the FDCS is due to the combination of the NN interaction and the binary collision mechanisms. This idea is further supported by the fact that a calculation performed at $q = 1$ a.u. for the case of the $2p$ orbital shows similar satellite peak structures as discussed for $2s$ in Fig. 8(c).

## IV. SUMMARY AND CONCLUSION

In this paper we applied the continuum distorted wave with eikonal initial-state approximation to describe ionization of Li under the impact of 6-MeV $H^+$ and 1.5-MeV/amu $O^{8+}$ ions. Doubly and fully differential cross sections have been evaluated within the framework of the independent electron

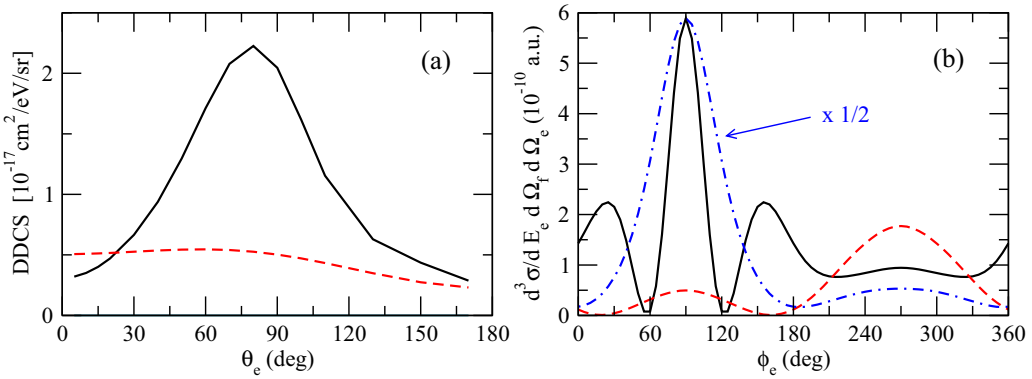


FIG. 11. (Color online) Differential cross section calculated in CDW-EIS for single ionization of $\mathrm{Li}(2s)$ by 1.5 MeV/amu $O^{8+}$ impact for $E_e = 1.5$ eV. (a) Doubly differential cross section as a function of $\theta_{el}$. (b) Fully differential cross section as a function of $\phi_{el}$ for fixed $q = 1.0$ a.u. and $\theta_e = 90^\circ$. Calculations including all (solid black) and only $l = 0,1$ (dashed red) partial waves in the expansion of the wave function of the ejected electron (see the text). In (b) the dashed-dotted blue line represents a calculation as that depicted by the solid line but without the NN interaction.

approximation. The effect of the internuclear interaction (NN) has been taken into account by a phase factor.

No importance of the NN interaction has been found for the case of proton projectiles. At the same time, when describing collisions with $O^{8+}$ ions the inclusion of the NN interaction potential in the calculation cannot be avoided for a proper account of the processes at play. The NN interaction potential is made by the Coulomb interaction of the heavy nuclei and two interaction terms due to the screening of the passive electrons and the polarization of the target by the incident projectile ion. The most dominant effect is provided by the Coulomb interaction term, however, the inclusion of the other potentials cannot be avoided for a proper account of the processes. A characteristic role of $V_{\rm pol}$ has been found in the DDCS for high $\eta$ values. $V_{\rm pol}$ is not uniquely defined for short distances and accordingly different approaches and different forms of $V_{\rm pol}$ are available in the literature. Three different forms of $V_{\rm pol}$ have been used in the present study and a very good reproduction of the measured DDCS has been obtained when $V_{\rm pol}$ is given by (6). $V_{\rm pol}$ of (6) depends on a cutoff parameter and its proper value might differ for the processes and systems under study. Note that we used $d = 0.57$ for our best results, while values for $d = 0.3$–$0.93$ have also been recommended in various studies in the field of electron-atom collisions [19–21]. In the case of the FDCS deviations in different forms of the NN interaction potential are more emphasized.

The satellite peak structure observed in the FDCS for the $O^{8+}$–Li($2s$) system was attributed to the nodal structure of the $2s$ orbital in [12] and [15]. Our study offers an alternative explanation, namely that the satellite structure is due to a combination of the NN interaction and the binary interaction mechanism.

## ACKNOWLEDGMENTS

This work was supported by the Natural Sciences and Engineering Research Council (NSERC) of Canada and by the Hungarian Scientific Research Fund (OTKA Grant No. K 109440). We thank E. Engel for making his atomic structure calculations available to us and D. Fischer for discussions on the data of Ref. [13].

[1] N. Stolterfoht, R. D. DuBois, and R. D. Rivarola, *Electron Emission in Heavy Ion-Atom Collisions* (Springer, Berlin, 1997).
[2] J. H. McGuire, *Electron Correlation Dynamics in Atomic Collisions* (Cambridge University Press, Cambridge, England, 1997).
[3] H. Schmidt-Böcking, V. Mergel, R. Dörner, H. J. Lüdde, L. Schmidt, T. Weber, E. Weigold, and A. Kheifets, *Many-Particle Quantum Dynamics in Atomic and Molecular Fragmentation*, Springer Series on Atomic, Optical and Plasma Physics Vol. 35, edited by J. Ullrich and V. P. Shevelko (Springer, Berlin, 2003), p. 353.
[4] J. Ullrich, R. Moshammer, A. Dorn, R. Dörner, L. P. H. Schmidt, and H. Schmidt-Böcking, Rep. Prog. Phys. **66**, 1463 (2003).
[5] M. Schulz, D. Fischer, R. Moshammer, and J. Ullrich, J. Phys. B: At. Mol. Opt. Phys. **38**, 1363 (2005).
[6] M. Schulz, M. F. Ciappina, T. Kirchner, D. Fischer, R. Moshammer, and J. Ullrich, Phys. Rev. A **79**, 042708 (2009).
[7] M. S. Schöffler, J. N. Titze, L. P. H. Schmidt, T. Jahnke, O. Jagutzki, H. Schmidt-Böcking, and R. Dörner, Phys. Rev. A **80**, 042702 (2009).
[8] D. Fischer, D. Globig, J. Goullon, M. Grieser, R. Hubele, V. L. B. de Jesus, A. Kelkar, A. LaForge, H. Lindenblatt, D. Misra *et al.*, Phys. Rev. Lett. **109**, 113202 (2012).
[9] M. Schulz, M. Dürr, B. Najjari, R. Moshammer, and J. Ullrich, Phys. Rev. A **76**, 032712 (2007).
[10] K. N. Egodapitiya, S. Sharma, A. Hasan, A. C. Laforge, D. H. Madison, R. Moshammer, and M. Schulz, Phys. Rev. Lett. **106**, 153202 (2011).
[11] S. Sharma, T. P. Arthanayaka, A. Hasan, B. R. Lamichhane, J. Remolina, A. Smith, and M. Schulz, Phys. Rev. A **89**, 052703 (2014).
[12] R. Hubele, A. LaForge, M. Schulz, J. Goullon, X. Wang, B. Najjari, N. Ferreira, M. Grieser, V. L. B. de Jesus, R. Moshammer *et al.*, Phys. Rev. Lett. **110**, 133201 (2013).
[13] A. C. LaForge, R. Hubele, J. Goullon, X. Wang, K. Schneider, V. L. B. de Jesus, B. Najjari, A. B. Voitkiv, M. Grieser, M. Schulz *et al.*, J. Phys. B: At. Mol. Opt. Phys. **46**, 031001 (2013).
[14] M. F. Ciappina, M. S. Pindzola, and J. Colgan, Phys. Rev. A **87**, 042706 (2013).
[15] H. R. J. Walters and C. T. Whelan, Phys. Rev. A **89**, 032709 (2014).
[16] D. S. F. Crothers and L. J. Dube, in *Advances in Atomic, Molecular, and Optical Physics*, edited by D. Bates and B. Bederson (Academic Press, San Diego, CA, 1992), Vol. 30, p. 287.
[17] C. J. Joachain, *Quantum Collision Theory* (North-Holland, Amsterdam, 1975).
[18] H. Nakanishi and D. M. Schrader, Phys. Rev. A **34**, 1810 (1986).
[19] X. Zhang, J. Sun, and Y. Liu, J. Phys. B: At. Mol. Opt. Phys. **25**, 1893 (1992).
[20] J. Mitroy, M. S. Safronova, and C. W. Clark, J. Phys. B: At. Mol. Opt. Phys. **43**, 202001 (2010).
[21] I. Y. Yurova and V. V. Kuverova, Russ. J. Phys. Chem. B **8**, 9 (2014).
[22] L. Gulyás, P. D. Fainstein, and A. Salin, J. Phys. B **28**, 245 (1995).
[23] L. Gulyás, A. Igarashi, P. D. Fainstein, and T. Kirchner, J. Phys. B: At. Mol. Opt. Phys. **41**, 025202 (2008).
[24] E. Engel and S. H. Vosko, Phys. Rev. A **47**, 2800 (1993).
[25] M. R. McDowell and J. P. Coleman, *Introduction to the Theory of Ion-Atom Collisions* (North-Holland, Amsterdam, 1970).
[26] P. D. Fainstein, L. Gulyás, and A. Salin, J. Phys. B: At. Mol. Opt. Phys. **29**, 1225 (1996).
[27] T. Kirchner, N. Khazai, and L. Gulyás, Phys. Rev. A **89**, 062702 (2014).
[28] J. C. Slater, Phys. Rev. **36**, 57 (1930).
[29] D. M. Schrader, Phys. Rev. A **20**, 918 (1979).
[30] C. Bottcher, J. Phys. B: At. Mol. Phys. **4**, 1140 (1971).
[31] A. B. Voitkiv and B. Najjari, Phys. Rev. A **79**, 022709 (2009).
[32] D. Fischer (private communication).